Propagation of three–dimensional Alfvén waves in a stratified, thermally conducting solar wind

S. Orlando[1], Y.-Q. Lou[2], R. Rosner[2], and G. Peres[1]

[1] Istituto ed Osservatorio Astronomico,
Piazza del Parlamento 1, 90134 Palermo, Italy

[2] Dept. of Astronomy & Astrophysics,
The University of Chicago, Chicago, IL 60637 USA

e-mail: orlando@oapa.astropa.unipa.it, lou@oddjob.uchicago.edu,
rrosner@oddjob.uchicago.edu, peres@oapa.astropa.unipa.it

Abstract

We model the propagation of three–dimensional, adiabatic, linear Alfvén waves in the solar atmosphere and wind, taking into account relevant physical effects, including gravity stratification, thermal conduction, radiative losses, and heating (via a phenomenological term). Our magnetohydrodynamic solar wind model also accounts for the momentum deposition by a spectrum of non–WKB Alfvén waves. The transmission and reflection of such waves has been previously studied by a variety of techniques, including calculations based on the computation of the ratio between the wavelength and the scale length of the Alfvén speed change and based on a globally – computed transmission coefficient. In this paper we discuss both techniques and show how they are related. We also discuss the physics underlying the reflection process and the possible role wave reflection might play in the acceleration of the solar wind and the winds from other stars.

1 Introduction

Since the early detection of Alfvén waves in the solar wind [*Belcher et al.*, 1969; *Belcher and Davis*, 1971] and the subsequent classic discussions [*Alazraki and Couturier*, 1971; *Belcher*, 1971; *Belcher and Olbert*, 1975; *Jacques*, 1977; *Hollweg*, 1973, 1978a; *Leer et al.*, 1982; *Holzer et al.*, 1983; *Rosner et al.*, 1986] it has been generally agreed that the interaction between Alfvén waves of solar origin and the ambient coronal gas is the most likely mechanism by which the solar wind is accelerated. As a result of recent high–latitude observations from the Ulysses spacecraft on the properties of the fast ($\gtrsim$ 700 km s^{-1}) solar wind [*Phillips et al.*, 1995; *Grall et al.*, 1996], the insignificant latitude variation of mean radial magnetic field, and the large–amplitude transverse magnetic field fluctuations [*Smith et al.*, 1995; *Balogh et al.*, 1995] there is a resurgent interest in the possible role of Alfvénic fluctuations in the acceleration of high–speed solar wind in addition to the well–known thermal expansion of the solar corona [*Parker*, 1958, 1963, 1991]. In particular, these transverse magnetic field fluctuations appear associated with outward propagating Alfvén waves [*Balogh et al.*, 1995]. Since the polar solar wind is observed to be remarkably steady without recurrent shear streams or other similar phenomena, the observed Alfvénic fluctuations in the polar solar wind most likely originate from the Sun.

In recent years there has been considerable new interest in Alfvén waves and compressible magnetohydrodynamic (MHD) waves in the solar atmosphere and wind as well as their nonlinear interactions with the background wind [*An et al.*, 1989, 1990; *Hollweg*, 1990, 1996; *Barkhudarov*, 1991; *Barnes*, 1992; *Similon and Zargham*, 1992; *Musielak et al.,*, 1992; *Velli*, 1993; *Lou*, 1992, 1993a, b, 1994a, b, 1995, 1996; *Rosner et al.,* 1991; *Lou and Rosner*, 1994; *MacGregor and Charbonneau*, 1994; *Krogulec et al.*, 1994; *Lau and Siregar,* 1996]. Nevertheless, while an enormous literature has grown on this subject, the theoretical details of exactly how this wave acceleration process takes place, and how it relates to the presence of solar high speed wind streams, remain uncertain. The reason for this difficulty is not a mystery: The fully general problem of exactly how finite amplitude Alfvén waves propagate and damp in the expanding, highly inhomogeneous, solar wind remains an extremely challenging computational problem and has not been fully solved as yet.

Recent work in this area has focused on the Alfvén wave propagation problem itself. As was first shown by *Ferraro* [1954] and *Ferraro and Plumpton* [1958], wave propagation is strongly affected by variations in the local Alfvén speed, so that, for example, waves may experience significant reflection across the transition region. Recently, *An et al.* [1989, 1990] and *Moore et al.* [1991] have pointed out that such wave reflection may play a very important role in the acceleration of the solar wind and, more generally, of stellar winds. To analyze the reflection of waves in the solar atmosphere, these authors compared the mode wavelength with the local scale height H_A of the Alfvén speed; by computing a critical angular frequency Ω_{cr}, *Musielak et al.,* [1992] argued that waves with frequency $\omega < \Omega_{cr}$ are evanescent (because their wavelength λ is larger than H_A), while waves with $\omega > \Omega_{cr}$ see the medium as approximatively uniform (because their wavelength is smaller than H_A). In other words, the Wentzel–Kramers–Brillouin (WKB) approximation is valid for waves with $\omega > \Omega_{cr}$.

While intuitively appealing, this approach is flawed, as has been pointed out by *Velli* [1993] (hereinafter referred to as V93) and *Hollweg* [1996]: V93 has noted that this approach is clearly local and is therefore unable to provide accurate predictions of wave propagation properties that depend upon the global nature of the atmosphere. Indeed, he proceeded to analyze the global propagation characteristics of Alfvén waves in both static and expanding isothermal atmospheres, defining the transmission coefficient through an inhomogeneous layer as the fraction of the energy flux able to propagate through such a layer.

In this paper we reconsider the propagation of the Alfvén waves through the solar atmosphere as discussed by V93, with three distinct aims: First, we seek to clarify the relation between the critical frequency approach and the transmission coefficient approach of V93; second, we would like to understand the physical reasons that determine the behavior of wave propagation as a function of wave frequency; third, we seek to extend the discussion of V93 to nonisothermal atmospheres. To this end we consider a background model that starts at the base of the transition region (with a temperature $T = 2 \times 10^4$ K), where the waves most likely originate. This model allows us to study the effects of the rapid increase of the Alfvén speed in the transition region on the wave propagation. Since wave reflection may play an important role in the wind acceleration, the wind model takes into account momentum deposition by a spectrum of non–WKB Alfvén waves. Since this model is not entirely self–consistent, as it neglects possible dissipative (damping) mechanisms for these waves (which could lead to heating of the corona), we consider adiabatic perturbations only, which do not dissipate energy into thermal energy of the background plasma. We account for the necessary heating by using a phenomenological heating term, since the heating process is not the object of study of this paper. We analyze the propagation properties of Alfvén waves in both a static and an expanding atmosphere.

The paper is structured as follows: In sections 2 and 3 we describe the solar wind background model and the wave equations, respectively; in sections 5 and 6 we discuss the propagation properties of the waves in the simplified scenario of a static atmosphere and in the presence of the wind, respectively; and finally, our summary and conclusions are found in section 7.

2 Background Stationary Wind

Throughout our analysis we adopt a spherical polar coordinate system (r, θ, ϕ). Since recent Ulysses observations indicate that $r^2 B$ does not vary appreciably with heliographic latitude [*Smith et al.*, 1995; *Balogh et al.*, 1995], we prescribe the radial magnetic field by

$$Br^2 = F_B \,, \tag{1}$$

where F_B is the constant magnetic flux. The equations for conservation of mass and momentum in spherical polar coordinates are written in the form [*Parker,* 1958; *Holzer,* 1977]

$$\rho u r^2 = F_M \,, \tag{2}$$

$$\rho u \frac{\partial u}{\partial r} = -\frac{\partial p}{\partial r} - \rho \frac{G M_S}{r^2} + \mathcal{P}_r \,, \tag{3}$$

where $\rho = \mu m_H n_p$ is the plasma mass density, $\mu = 1.268$ is the mean atomic mass for solar abundances, m_H is the hydrogen atom mass, n_p is the proton number density, u is the radial plasma flow speed, F_M is the (fixed) mass flux, $p = 2.2 n_p k_B T$ is the pressure, k_B is the Boltzmann constant, T is the temperature, G is the gravitational constant, M_S is the solar mass, and $\mathcal{P}_r$ is the contribution of momentum addition rate per unit volume due to Alfvén waves (which will be discussed in the next section). The equation describing the energy balance is

$$\frac{\rho^\gamma}{\gamma - 1} u \frac{\partial}{\partial r}\left(\frac{p}{\rho^\gamma}\right) - \frac{1}{r^2}\frac{\partial}{\partial r}\left(r^2 \kappa \frac{\partial T}{\partial r}\right) = H - \frac{p^2}{4.84 k_B^2 T^2}\Lambda(T) \,, \tag{4}$$

where $\gamma = 5/3$ is the ratio of specific heats, $\kappa = 9.2 \times 10^{-7} T^{5/2}$ is the thermal conductivity in cgs units given by *Spitzer* [1962], H is the volumetric heat input rate, and $\Lambda(T)$ is the radiative loss per unit emission measure [*Raymond and Smith,* 1977]. In light of our ignorance of the specifics about the coronal heating mechanism [*Parker,* 1991] we have chosen for H the parameterized form [*Rosner et al.,* 1978]

$$H = \frac{H_S R_S^2}{r^2}\, e^{-(r - R_S)/\lambda_H} \,, \tag{5}$$

where H_S is the volumetric heating rate at the base of the transition region and λ_H is the heating scale length. We reemphasize that in this paper we do not separately consider energy deposition by dissipation of the Alfvén waves; i.e., we assume the MHD perturbations to be adiabatic (in other words, there is no dissipation of Alfvén wave energy into thermal energy of the plasma). On the other hand, exchange of mechanical and magnetic energies does occur; i.e., the waves do work on the plasma, as was extensively discussed by *Lou* [1993a].

3 Three–Dimensional Alfvén Wave Equations

Lou [1993a] considered the propagation of three–dimensional (3–D), adiabatic MHD perturbations in a spherically symmetric, radial solar wind background. In the linear approximation he showed that the 3–D propagation of the Alfvén waves decouples from the 3–D propagation of the compressible MHD fast and slow waves in the wind [*Lou,* 1993b]; the Alfvén wave equations can then be expressed in the form

$$\frac{\partial j}{\partial t} = \frac{1}{r^2}\frac{\partial}{\partial r}(r^2 B \xi) - \frac{1}{r^2}\frac{\partial}{\partial r}(r^2 u j) \,, \tag{6}$$

$$\frac{\partial \xi}{\partial t} + \frac{u}{r^2}\frac{\partial}{\partial r}(r^2 \xi) = \frac{B}{4\pi\rho r^2}\frac{\partial}{\partial r}(r^2 j) \,, \tag{7}$$

where t is the time, and

$$j \equiv \frac{1}{r \sin\theta}\left[\frac{\partial(\sin\theta\, b_\phi)}{\partial \theta} - \frac{\partial b_\theta}{\partial \phi}\right] \,, \tag{8}$$

$$\xi \equiv \frac{1}{r\sin\theta}\left[\frac{\partial(\sin\theta v_\phi)}{\partial\theta} - \frac{\partial v_\theta}{\partial\phi}\right] ; \tag{9}$$

where j is proportional to the r component of the electric current density perturbation and ξ is the r component of the vorticity perturbation. The quantities b_ϕ, b_θ are the angular components of the transverse magnetic field perturbation $\mathbf{b}_\perp$, and v_ϕ, v_θ are the angular components of the transverse velocity perturbation $\mathbf{v}_\perp$. Following the standard procedure for separation of variables, and assuming a $Y_{lm}(\theta,\phi)\exp(i\omega t)$ functional form for both $j(r,\theta,\phi,t)$ and $\xi(r,\theta,\phi,t)$, where $Y_{lm}(\theta,\phi)$ is the spherical harmonic function with degrees l and m, we can express the general 3–D solution of (6) and (7) in the form [*Lou,* 1993a]

$$j(r,\theta,\phi,t) = \sum_{lm}\int_{-\infty}^{\infty} d\omega\; a_{lm}(\omega) j_\omega(r) Y_{lm}(\theta,\phi)\exp(i\omega t)\,, \tag{10}$$

$$\xi(r,\theta,\phi,t) = \sum_{lm}\int_{-\infty}^{\infty} d\omega\; a_{lm}(\omega) \xi_\omega(r) Y_{lm}(\theta,\phi)\exp(i\omega t)\,, \tag{11}$$

where the $\{a_{lm}(\omega)\}$ represents a set of complex coefficients which depend only on ω. For real $j(r,\theta,\phi,t)$ and $\xi(r,\theta,\phi,t)$ these coefficients have the property that $a_{lm}(\omega) = (-1)^m a^\dagger_{l,-m}(-\omega)$, where the dagger denotes the complex conjugation.

The angular components of the transverse magnetic field perturbation and of the transverse velocity perturbation are determined from the conditions of zero transverse magnetic and velocity divergence perturbations, namely, $\nabla_\perp\cdot\mathbf{b}_\perp = 0$ and $\nabla_\perp\cdot\mathbf{v}_\perp = 0$, and from the definitions (8) and (9) for j and ξ,

$$b_\theta(r,\theta,\phi,t) = \sum_{lm}\int_{-\infty}^{\infty} d\omega\,\frac{imr j_\omega(r) a_{lm}(\omega)}{l(l+1)}\frac{Y_{lm}(\theta,\phi)}{\sin\theta}\exp(i\omega t) \tag{12}$$

$$b_\phi(r,\theta,\phi,t) = -\sum_{lm}\int_{-\infty}^{\infty} d\omega\,\frac{r j_\omega(r) a_{lm}(\omega)}{l(l+1)}\frac{\partial Y_{lm}(\theta,\phi)}{\partial\theta}\exp(i\omega t) \tag{13}$$

$$v_\theta(r,\theta,\phi,t) = \sum_{lm}\int_{-\infty}^{\infty} d\omega\,\frac{im\; r\xi_\omega(r) a_{lm}(\omega)}{l(l+1)}\frac{Y_{lm}(\theta,\phi)}{\sin\theta}\exp(i\omega t) \tag{14}$$

$$v_\phi(r,\theta,\phi,t) = -\sum_{lm}\int_{-\infty}^{\infty} d\omega\,\frac{r\xi_\omega(r) a_{lm}(\omega)}{l(l+1)}\frac{\partial Y_{lm}(\theta,\phi)}{\partial\theta}\exp(i\omega t) \tag{15}$$

with $l \geq 1$.

Energy conservation for the three–dimensional propagation of Alfvén waves in the solar wind can be expressed in the form

$$\frac{\partial\epsilon}{\partial t} + \nabla\cdot\mathcal{E} = -u\mathcal{P}_r\,, \tag{16}$$

where ϵ and $\mathcal{E}$ are the energy density and the radial energy flux density, respectively, of the Alfvénic perturbation, defined as [*Lou,* 1993a]

$$\epsilon = \frac{\rho(v_\theta^2+v_\phi^2)}{2} + \frac{(b_\theta^2+b_\phi^2)}{8\pi}\,, \tag{17}$$

$$\mathcal{E} = \rho u\frac{(v_\theta^2+v_\phi^2)}{2} + u\frac{(b_\theta^2+b_\phi^2)}{4\pi} - B\frac{(b_\theta v_\theta + b_\phi v_\phi)}{4\pi}\,. \tag{18}$$

The right-hand side of (16) is not zero but represents the power loss per unit volume due to the MHD wind acceleration. The time–averaged wave force density is expressed as

$$\mathcal{P}_r = \frac{\rho(v_\theta^2 + v_\phi^2)}{r} - \frac{(b_\theta^2 + b_\phi^2)}{4\pi r} - \frac{\partial}{\partial r}\left(\frac{b_\theta^2 + b_\phi^2}{8\pi}\right) , \tag{19}$$

where the first two terms are the centrifugal and the magnetic tension force densities, respectively, and the third term is the gradient of the magnetic pressure [*MacGregor and Charbonneau*, 1994]. It is worth noting that the centrifugal and the magnetic tension components cancel each other in the WKB limit (i.e., the high–frequency regime [*Hollweg*, 1973]), so that the wave force density is due to the magnetic pressure alone [*Parker*, 1965; *Alazraki and Couturier*, 1971; *Belcher*, 1971]. This approximation is valid if the propagation speed V_A does not vary appreciably over a wave period, so that the waves propagate without reflection. Since our background model includes the transition region (where the Alfvén speed increases rapidly with height [see *Similon and Zargham*, 1992]), we expect significant wave reflection there [*Ferraro*, 1954] and hence a nonnegligible contribution from the centrifugal and the magnetic tension components. In order to consider a partially self–consistent solar wind model we include in the momentum equation (3) the effects of Alfvén wave propagation in the non–WKB regime.

The detailed expression for $\mathcal{P}_r$ due to the three–dimensional propagation of Alfvén waves in the solar wind can be found in the paper by *Lou* [1993a]. Substituting the first–order Alfvén wave solutions (6)–(15) in (19) gives the r component of the wave momentum source term as

$$\begin{aligned}\mathcal{P}_r \;=\; & \sum_{\substack{l_1 m_1 \\ l_2 m_2}} \int\!\!\int d\omega_1 d\omega_2 \frac{a_{l_1 m_1}(\omega_1) a_{l_2 m_2}(\omega_2) \exp\left[i(\omega_1+\omega_2)t\right]}{l_1(l_1+1) l_2(l_2+1)} \\ & \times \left[\rho r \xi_{\omega_1}\xi_{\omega_2} - \frac{j_{\omega_1}}{4\pi}\frac{\partial}{\partial r}(r^2 j_{\omega_2})\right] \left(\frac{\partial Y_{l_1 m_1}}{\partial\theta}\frac{\partial Y_{l_2 m_2}}{\partial\theta} - \frac{m_1 m_2 Y_{l_1 m_1} Y_{l_2 m_2}}{\sin^2\theta}\right) ,\end{aligned} \tag{20}$$

where $\xi_\omega(r)$ and $j_\omega(r)$ are the radial solutions of (6) and (7) at a given angular frequency ω and $a_{lm}(\omega)$ represents the complex amplitude for both $j_\omega(r) Y_{lm}(\theta,\phi)\ \exp(i\omega t)$ and $\xi_\omega(r) Y_{lm}(\theta,\phi)$ $\exp(i\omega t)$. Both steady and unsteady components are present in this radial momentum source term; the former drives secondary MHD flows, while the latter drives secondary MHD waves. Our interest here focuses on the acceleration of the (steady) wind; we therefore consider only the steady component in (20), which is the result of nonlinear self–coupling of each frequency component, that is, those components with $\omega_2 = -\omega_1$. We note also that the radial and the angular dependences are separated for each individual term in the summation (20). Since we integrate the wind and the wave equations radially, we may regard the angular dependence as an arbitrary parameter $\mathcal{Q}_\omega(\theta,\phi)$ for any given ranges of l, m and for any given set of complex amplitudes $a_{lm}(\omega)$; the typical momentum deposition from each individual term is in the form of

$$\mathcal{P}_r = \int d\omega \left[\rho r \xi_\omega \xi_{-\omega} - \frac{j_\omega}{4\pi}\frac{\partial}{\partial r}(r^2 j_{-\omega})\right] \mathcal{Q}_\omega(\theta,\phi) . \tag{21}$$

To compute $\mathcal{P}_r$, we have considered an illustrative input spectrum of Alfvén waves at the base of the transition region, with periods in the range 5×10^{-3} to 3×10^2 hours, where most of the observed energy due to the propagating disturbances lies [e.g., *Coleman*, 1968; *Roberts and Goldstein*, 1991; *Goldstein et al.,*, 1995; *Tu and Marsch*, 1995]; we have assumed that at the transition region base, $\mathcal{Q}_\omega(\theta,\phi) \propto \omega^{-1.6}$, where the spectral index 1.6 lies in the observed range 1.5–1.7. The "emergent" spectrum, i.e., the resulting spectrum at large heliocentric distances, will be discussed below. The integral over frequencies in (21) is now approximated by a sum over 10 discrete frequencies,

$$\mathcal{P}_r = \mathcal{K}\sum_{k=1}^{10} \omega_k^{-1.6} \left[\rho r \xi_{\omega_k}\xi_{-\omega_k} - \frac{j_{\omega_k}}{4\pi}\frac{\partial}{\partial r}(r^2 j_{-\omega_k})\right] , \tag{22}$$

where $\mathcal{K}$ is a constant derived with the method discussed in the next section, and the 10 chosen frequencies are

$$\omega_k/2\pi = 10^{-6},\ 5\times10^{-6},\ 10^{-5},\ 5\times10^{-5},\ 10^{-4},$$
$$5\times10^{-4},\ 10^{-3},\ 5\times10^{-3},\ 10^{-2},\ 5\times10^{-2}\ \text{Hz}\ . \tag{23}$$

4 Numerical Techniques

The wave and wind equations are coupled through the term for the deposition rate of wave momentum density in (3). To obtain a joint solution of these coupled equations, we have adopted a solution procedure similar to that used by *MacGregor and Charbonneau* [1994]:

1. We integrate the wind equations (3), (4), and (5), using a standard fourth–order Runge–Kutta method with adaptive stepsize control (by step doubling) [*Press et al.,* 1986]. We assign the boundary conditions at the base (i.e., temperature, proton number density, radial flow velocity, and heat flux) and then iterate on the base radial flow velocity in order to find the transonic solution. We adopt the WKB approximation in order to compute the wave momentum deposition,

$$(\mathcal{P}_r)_{\text{WKB}} = -\frac{\partial}{\partial r}\left(\frac{b_\theta^2 + b_\phi^2}{8\pi}\right) , \tag{24}$$

and we assume the WKB Alfvén wave amplitudes at the base of the transition region $(\mathbf{b}_{\perp S}^2)_{\text{WKB}} = 10^{-3} B_S^2$.

2. Adopting the resulting profiles for the physical variables of the magnetized background wind, we integrate the Alfvén wave equations (6) and (7), using the Henyey method relaxation scheme [*Henyey et al.,* 1964], on the basis of the Newton–Raphson iterative procedure [*Press et al.,* 1986]. The choice of a relaxation method over a fourth–order Runge–Kutta shooting method to integrate the Alfvén wave equations is motivated by the desire to avoid burdensome interpolation of physical quantities which characterize the solar atmosphere and wind at each integration step of the wave equations.

3. We compute the non–WKB time–averaged wave force density due to a spectrum of Alfvén waves from (22). We impose $\mathcal{P}_{rS} = (\mathcal{P}_{rS})_{\text{WKB}}$ at the base of the transition region to compute the constant $\mathcal{K}$ in (22). For the wind model discussed in the present paper, $\mathcal{K} = 1.8 \times 10^{-7}$.

4. We return to solve the wind equations (3), (4), and (5) again, but now using the wave force density obtained in the previous step; this approach allows us to update the physical wind quantities so that they are (more) consistent with the wave momentum deposition.

5. We iterate on steps 2–4 until the wind solution converges according to a predetermined criterion: We monitor the convergence by examining the values of the base radial flow velocity u_S, the base volumetric heating rate H_S, and the Alfvén critical point r_A, and we stop the iteration process when the relative variation of each of these quantities in two successive iterations is less than 0.01%. It is worth noting that H_S is adjusted in each iteration so as to have a wind temperature $T = 5\times10^5$ K at ~ 1 AU.

5 Propagation Through a Static Solar Atmosphere

Alfvén waves undergo strong reflection whenever the gradient of the Alfvén speed is very steep. One expects very significant reflection in the transition region due to the sudden change of the temperature and density in this layer [*Ferraro*, 1954]. Because this layer is very close to the solar surface, the radial wind speed there should be very subsonic; for this reason it is not entirely unreasonable to begin our analysis by assuming a static atmosphere, even though our ultimate aim is to understand the transmission of Alfvén waves in the solar wind. Various aspects of this simplified model problem have been considered earlier [*Hollweg*, 1978b; *Leroy*, 1980; *Rosner et al.*,, 1986; *An et al.*, 1990; *Similon and Zargham*, 1992; V93; *Lou and Rosner*, 1994]. This approach also allows us to clarify the physics leading to wave reflection in the simplest of possible (nontrivial) models and furthermore gives us a way of distinguishing the unique physical effects of the flow on the wave propagation from effects due to other causes (such as stratification).

For our purposes we consider a static background solar atmosphere described by the energy balance relation between the thermal conduction, radiative losses, and volumetric heating rate (see (4)) and by the equation of hydrostatic equilibrium,

$$\frac{\partial p}{\partial r} = -\rho \frac{GM_S}{r^2} + \mathcal{P}_r \; ; \tag{25}$$

that is, the radial flow term on the left-hand side of (3) is dropped. The magnetic field is taken to be radial and monopolar, that is, $B = F_B/r^2$ with a constant F_B, so as to mimic a diverging magnetic field geometry in a coronal hole.

In a static background the Alfvén wave equations (6) and (7) become

$$\frac{\partial j}{\partial t} = B \frac{\partial \xi}{\partial r} , \tag{26}$$

$$\frac{\partial \xi}{\partial t} = \frac{V_A^2}{Br^2} \frac{\partial (r^2 j)}{\partial r} , \tag{27}$$

where $V_A = B/(4\pi\rho)^{1/2}$ is the Alfvén speed and where we have used $Br^2 = F_B$ in (26). The above Alfvén wave equations can be expressed in the nondimensional form as

$$\frac{\partial \overline{j}}{\partial \overline{t}} = \frac{1}{\overline{r}^2} \frac{\partial \overline{\xi}}{\partial \overline{r}} , \tag{28}$$

$$\frac{\partial \overline{\xi}}{\partial \overline{t}} = \overline{V}_A^2 \frac{\partial (\overline{r}^2 \overline{j})}{\partial \overline{r}} , \tag{29}$$

where $\overline{j} = jR_S/B_S$, $\overline{\xi} = \xi R_S/V_{AS}$, $\overline{r} = r/R_S$, $\overline{t} = tV_{AS}/R_S$, $\overline{V}_A = V_A/V_{AS}$, and the subscript S denotes quantities evaluated at the base of the transition region. Assuming the temporal variation $\exp(i\overline{\omega}\overline{t})$ for both $\overline{j}$ and $\overline{\xi}$, where $\overline{\omega} = \omega R_S/V_{AS}$ is the nondimensional angular frequency, equations (28) and (29) can be readily combined to form a single second–order ordinary differential equation for $\overline{\xi}$, namely,

$$\frac{d^2\overline{\xi}}{d\overline{r}^2} + \frac{\overline{\omega}^2}{\overline{V}_A^2} \overline{\xi} = 0 \; . \tag{30}$$

It is fairly straightforward to obtain numerical Alfvén wave solutions from (30).

The next step is to compute the wave transmission coefficient $\mathcal{T}$ for the transition region and inner corona. Because of the nonzero gradient of the Alfvén speed in these regions, inward and outward propagating waves are coupled [*Heinemann and Olbert,* 1980], so that an outward propagating wave generates incoming waves, which in turn generate outgoing waves. As a consequence an initial wave train generates an infinite sequence of outward and inward propagating wave trains, which modify the initial wave train itself, making it impossible to distinguish between transmitted, reflected, and incident waves. In order to surmount this problem, and so to uniquely define a transmission coefficient through a stratified layer, *Leroy* [1980] adopted the artifice of assuming that the layer under consideration was bounded on both sides by homogeneous media, which are characterized by a uniform Alfvén speed. With this assumption the (uncoupled) outward and inward propagating waves in the medium directly below the layer under study can be unambiguously associated with the incident and the reflected waves, respectively, while in the medium above the layer of interest the outward propagating wave corresponds unambiguously to the transmitted wave. As will be shown below, this trick does introduce some small anomalies into the solutions, but these turn out to be sufficiently minor (and do not affect the principal conclusions regarding the physics) that they may be neglected.

In our case we are interested in the propagation of the Alfvén waves through the transition region and the corona. Following *Lou and Rosner* [1994] (hereinafter LR94) and in the spirit of *Leroy*'s [1980] treatment, we place a homogeneous medium below the base of the transition region and assume that the uniform Alfvén speed in this base layer is equal to the Alfvén speed at the base of the transition region. We can interpret this medium as the source region for the waves; this artifice allows us to distinguish between the incident and the reflected waves at the base of the transition region. Unfortunately, this trick does not work in the outer region, because it is quite unrealistic to assume an analogous homogeneous medium above some arbitrary height in the corona—the solar atmosphere is intrinsically inhomogeneous everywhere. To solve this problem, *Hollweg* [1978b] proposed a weaker assumption, which proves useful here: If the WKB approximation is valid at some heliocentric distance $r_{\rm WKB}$, no reflections are expected to appear in the medium beyond $r_{\rm WKB}$, and the outward propagating wave can be effectively considered as the transmitted wave. We therefore assume that the Alfvén waves are not reflected far enough (i.e., $r > r_{\rm WKB}$) from the Sun.

With the above assumption borne in mind, it is now straightforward to compute the transmission coefficient $\mathcal{T}$. We have adopted two different methods to do this in order to check our results. The first method uses (like V93) the conservation of the net wave energy flux in a static background [*Bray and Loughhead*, 1974], which can be written in the spherical coordinates as

$$\mathcal{E}^+ - \mathcal{E}^- = \mathcal{E}_\infty \ , \qquad \mathcal{E}^\pm = \rho r^2 V_A \frac{|\mathbf{z}^\pm|^2}{8} \ , \tag{31}$$

where the plus and minus sign indicate the outward and inward directed radial wave energy fluxes, respectively, $\mathcal{E}_\infty$ is a constant, and

$$\mathbf{z}^\pm = \mathbf{v}_\perp \mp \mathrm{sgn}(B)\mathbf{b}_\perp/\sqrt{4\pi\rho}$$

are the Elsässer variables [*Elsässer,* 1950].

The transmission coefficient $\mathcal{T}$ across an atmospheric layer bounded by regions of constant Alfvén speed (or by regions with negligible reflection) is correctly defined as the fraction of the initially outward propagating energy flux at the atmospheric base which reaches the region in which the WKB approximation is valid (hereinafter referred to as the WKB region), namely,

$$\mathcal{T} = \mathcal{E}^+_{\rm WKB}/\mathcal{E}^+_S \ , \tag{32}$$

where $\mathcal{E}^+_{\rm WKB}$ is the outward propagating energy flux in the WKB region and $\mathcal{E}^+_S$ is the outward propagating energy flux at the atmospheric base. If we impose the boundary condition that only outward propagating waves exist in the WKB region and beyond, then $\mathcal{E}^+_{\rm WKB} = \mathcal{E}_\infty$.

An alternative way to compute the transmission coefficient is analogous to that used by LR94, described as follows. If the Alfvén speed is uniform below the base of the transition region and equal to its value at the base of the transition region, then $\overline{V}_A = \overline{V}_{AS} = 1$ in (30), and one can write the general analytical solution of this equation,

$$\overline{\xi} = \mathcal{A}e^{-ik\overline{r}} + \mathcal{B}e^{ik\overline{r}} , \tag{33}$$

where the dimensionless radial wavenumber $k = \overline{\omega}$. We then match these solutions to the numerical solutions for the inhomogeneous overlying atmosphere, corresponding to an outgoing Alfvén wave far above the solar surface: We require that $\overline{\xi}$ and its radial derivative $\overline{\xi}'$ be continuous at the base of the transition region. These two conditions allow us to obtain the reflection coefficient $\mathcal{R}$ (and thus the transmission coefficient $\mathcal{T}$ from the conservation law $\mathcal{T} + \mathcal{R} = 1$) at the base of the transition region,

$$\mathcal{R} = \frac{|\overline{\xi}'_S|^2 + k^2|\overline{\xi}_S|^2 + 2k\Im\left[\overline{\xi}^\dagger_S\overline{\xi}'_S\right]}{|\overline{\xi}'_S|^2 + k^2|\overline{\xi}_S|^2 - 2k\Im\left[\overline{\xi}^\dagger_S\overline{\xi}'_S\right]} , \tag{34}$$

where $\overline{\xi}_S$ and $\overline{\xi}'_S$ are, respectively, $\overline{\xi}$ and $\overline{\xi}'$ computed at the base of the transition region, and where the dagger represents the complex conjugation.

Following the above scheme, we integrate (30) by imposing the boundary conditions sufficiently far from the Sun that the assumption that the solution there corresponds to an outward propagating WKB wave is reasonable. For an isothermal static atmosphere, LR94 obtained analytical solutions to equations (28) and (29) at sufficiently large distances from the Sun. In order to use their analytical forms we consider temperature profiles that are practically isothermal and without the Alfvén wave momentum deposition for heliocentric distances larger than $R_* \sim 6\ R_S$. Our boundary conditions for $\overline{j}$ and $\overline{\xi}$, corresponding to an outward propagating Alfvén wave far from the Sun, are

$$\begin{aligned} \overline{j} \;&=\; a_\circ \frac{4R_\odot H_p^2}{B_\odot R_*^4} e^{i\overline{\omega}\overline{t}} \times \left[x^{-1} + \frac{1}{2}x^{-2} + \frac{1}{8}x^{-3} + \left(\frac{1}{48} - \frac{2i}{3\vartheta}\right) x^{-4} \right. \\ &\left. + \left(\frac{1}{384} + \frac{2i}{3\vartheta}\right) x^{-5} + \cdots \right] \times \exp\left(-i\vartheta \int x^2 e^{1/x} dx\right) , \end{aligned} \tag{35}$$

$$\begin{aligned} \overline{\xi} \;&=\; -a_\circ \frac{4R_\odot H_p^2}{B_\odot R_*^4} \left(\frac{\rho_\odot}{\rho_*}\right)^{1/2} \exp[R_*/(2H_p)] e^{i\overline{\omega}\overline{t}} \times \left[x^{-1} - \frac{1}{2}x^{-2} + \frac{1}{8}x^{-3} \right. \\ &\left. - \left(\frac{1}{48} - \frac{i}{3\vartheta}\right) x^{-4} + \left(\frac{1}{384} - \frac{2i}{3\vartheta}\right) x^{-5} + \cdots \right] \times \exp\left(-i\vartheta \int x^2 e^{1/x} dx\right) , \end{aligned} \tag{36}$$

where

$$\int x^2 e^{1/x} dx = \frac{1}{6}\left[(2x^3 + x^2 + x) \exp\left(\frac{1}{x}\right) + \ln x - \sum_{n=0}^{\infty} \frac{x^{-(n+1)}}{(n+1)!(n+1)} \right] , \tag{37}$$

and where $H_p = [k_B T_*/(\mu m_H)]/(GM_S/R_*^2)$ is the pressure scale height at $r = R_*$, ρ_* and T_* are the mass density and temperature, respectively, at $r = R_*$, $a_\circ$ is a constant coefficient, the dimensionless radial coordinate $x \equiv 2H_p r/R_*^2$, and the square of the dimensionless angular frequency (LR94)

$$\vartheta^2 \equiv \omega^2 \pi \rho_* \exp(-R_*/H_p)(R_*^2/H_p)^6/(16F_B^2).$$

The adopted parameters of the static background model are typical of solar conditions in a coronal hole; the values of temperature, proton number density, magnetic field strength, volumetric heating rate at the base of the transition region, heating scale length and maximum temperature $T_{max} \equiv T_*$ are summarized in Table 1. This table also contains the parameters characterizing the background wind model, discussed in the next section.

We have integrated the Alfvén wave equation (30), using boundary conditions (35) and (36) sufficiently far above the solar surface (so that the WKB approximation is valid). The transmission coefficient $\mathcal{T}$ is obtained as a function of the dimensionless angular wave frequency $\bar{\omega}$, using both methods described above, and is shown (solid line) in Figure 1 as a function of the dimensional wave period in hours. The dashed line indicates a rough estimate of the transmission coefficient $\mathcal{T}$, as discussed below. We also mark the nondimensional angular frequency $\bar{\omega}$ along the upper horizontal axis in Figure 1. A strong dependence of wave transmission on the wave period is evident for periods longer than ~0.1 s, while waves with periods shorter than 0.1 s are completely transmitted through the model solar atmosphere. The wave transmission reaches a minimum at a period of $\sim$ 1 hour and a maximum at a longer period. Finally, the wave transmission shows a decrease with $\overline{\omega}$ at longer periods and tends to zero for $\overline{\omega} \to 0$.

This behavior can be better understood with the aid of the critical frequency introduced by Musielak and coworkers [*Musielak et al.*, 1992]. These authors showed that the equations for Alfvén waves in a static background can be cast into the Klein–Gordon form (for a similar transformation in spherical geometry, see LR94); and they suggested that the coefficient of the zeroth–order term in the Klein–Gordon equations could be regarded as a kind of potential barrier to wave propagation. Nevertheless, the Klein–Gordon forms of equations associated with transverse velocity and magnetic field perturbations actually involve two different "potential barriers"; if equations (26) and (27) are recast so that the barrier terms have coefficients with the dimension of frequency squared, then these two barriers (with subscripts minus and plus) are

$$\Omega_{\mp}^2 = \left(\frac{V_{AS}}{R_S}\right)^2 \left[\left(\frac{1}{2}\frac{d\overline{V}_A}{d\overline{r}}\right)^2 \mp \frac{\overline{V}_A}{2}\frac{d^2\overline{V}_A}{d\overline{r}^2} \right], \tag{38}$$

respectively (see Figure 2). Formally, both Ω_-^2 and Ω_+^2 can be positive or negative in a given radial range. The question then arises as to which one should be used to define an effective local critical frequency. On the basis of heuristic arguments and (38), *Musielak et al.* [1992] proposed to introduce the following quantity as an estimate for the local critical frequency,

$$\Omega_{cr} = \frac{V_{AS}}{R_S} \left[\left(\frac{1}{2}\frac{d\overline{V}_A}{d\overline{r}}\right)^2 + \frac{\overline{V}_A}{2}\left|\frac{d^2\overline{V}_A}{d\overline{r}^2}\right| \right]^{1/2}, \tag{39}$$

such that waves with angular frequencies less than Ω_{cr} are reflected by the medium (see Figure 2; see also LR94). Figure 3 shows the variations of the Alfvén speed V_A (top) and the nondimensional critical frequency $\overline{\Omega}_{cr} = \Omega_{cr} R_S / V_{AS}$ (bottom) as functions of the heliocentric distance $\overline{r}$ for our model solar atmosphere. It is evident that the critical frequency decreases with increasing radial distance from the Sun. As a consequence, a wave with a given angular frequency ω will propagate freely after some distance r_ω from the Sun, this distance being farther out the lower the ω is; in other words, the thickness $\delta \equiv r_\omega - R_S$ of the evanescence layer, in which the wave frequency is less than Ω_{cr}, increases with decreasing frequency. As an aside we note that matching the static atmosphere with the isothermal layer (discussed just above) introduces a small "wiggle" in the transmission coefficient $\mathcal{T}$ close to the transmission coefficient minimum (cf. Figure 1; the small discontinuity near $\bar{r} \sim 6$ in critical frequencies seen in Figures 2 and 3 is associated with this artifact). As can be seen, this artifact is sufficiently small not to affect the substance of the solution.

To evaluate the transmission coefficient $\mathcal{T}$, we shall invoke a simplifying approximation, which can help to understand the result of the more complex detailed calculation. Suppose that for a given frequency the thickness δ is much smaller than the wavelength λ, so that the wave sees the variation of the propagation speed as a discontinuity. In this case the transmission coefficient $\mathcal{T}$ can be roughly estimated by

$$\mathcal{T} = \frac{4 V_{AS} V_{A\omega}}{(V_{AS} + V_{A\omega})^2}, \tag{40}$$

where $V_{A\omega}$ is the Alfvén speed at r_ω. Although this approximation is, strictly speaking, incorrect if λ is of the order of, or smaller than, δ, we will nevertheless use it to compute the transmission coefficient for all frequencies. (It turns out that the resulting error for the "inappropriate" frequencies is remarkably small.) The result is shown as the dashed curve in Figure 1. Note that its behavior is very similar to that of the solid curve computed by using the more detailed (and correct) procedures. In particular, the results all scale in the same way at low and high frequencies, and their maximum and the minimum are located at approximatively the same frequencies.

These results allow us to clarify the physics underlying the maximum and minimum found in the transmission coefficient curve. Consider first the bottom panel of Figure 3: As the frequency ω is increased from zero, the point r_ω where transmission can occur moves inward, so that the thickness of the evanescent region, δ, decreases, and (as shown in the upper panel) the Alfvén speed $V_{A\omega}$ increases. The transmission coefficient estimated by (40) therefore increases from zero and reaches its maximum value (equal to one) when $V_{A\omega} = V_{AS}$. As the frequency is further increased, $V_{A\omega}$ continues to increase and eventually becomes larger than V_{AS}; the transmission coefficient therefore decreases, reaching its minimum value when the Alfvén speed is maximum. For yet higher frequencies the Alfvén speed decreases and the transmission again increases, becoming of the order of unity (e.g., totally transmitting) for frequency higher than the maximum critical frequency $\overline{\Omega}_{cr} \sim 10^5$ (cf. lower panel in Figure 3).

Thus we see that the maximum in the transmission coefficient $\mathcal{T}$ at low frequencies occurs because the values of the propagation velocities at the two boundaries of the evanescent layer are very close; the value of $\mathcal{T}$ at this maximum is, however, significantly lower than the value predicted by (40). The reason for this discrepancy is easily understood: The thickness of the evanescent layer is not much smaller than the wavelength λ (as required by the approximation leading to (40)), so that although $V_{A\omega} = V_{AS}$, wave reflection nevertheless occurs because of the inhomogeneous profile of V_A within this layer itself.

The transmission minimum at intermediate frequencies is, in contrast, a consequence of the maximum in the Alfvén speed. On the basis of this argument we would expect that this minimum becomes more prominent as the difference between the maximum Alfvén speed and the base Alfvén speed increases; this is in fact observed in our detailed calculations.

6 Propagation in the Solar Wind

In this section we focus on the propagation of Alfvén waves in the solar wind, that is, in an expanding background atmosphere. The wind background is described by (1)–(5), while the equations for Alfvén wave propagation are (6) and (7).

As in the static case we rewrite the wave equations in a nondimensional form and assume that the functional form of the time dependence of wave solutions is given by $\exp(\overline{\sigma}\overline{t})$, where $\overline{\sigma} = i\omega R_S/V_{AS}$ is purely imaginary and V_{AS} is the Alfvén speed at the base of the transition region; the resulting equations are then

$$\frac{1}{\overline{r}^2}\left(1-\frac{\overline{u}^2}{\overline{V}_A^2}\right)\frac{d\overline{\xi}}{d\overline{r}} = M_{AS}\left(\overline{\sigma}+\frac{2\overline{u}}{\overline{r}}\right)\overline{\xi} + \left(\overline{\sigma}+\frac{d\overline{u}}{d\overline{r}}\right)\overline{j}, \tag{41}$$

$$\overline{u}\frac{d\overline{j}}{d\overline{r}} = M_{AS}\overline{u}\frac{d\overline{\xi}}{d\overline{r}} + M_{AS}\left(\overline{\sigma}+\frac{2\overline{u}}{\overline{r}}\right)\overline{\xi} - \frac{2\overline{u}}{\overline{r}}\overline{j}, \tag{42}$$

where, as before, $\overline{j} = jR_S/B_S$, $\overline{\xi} = \xi R_S/V_{AS}$, $\overline{r} = r/R_S$, $\overline{t} = tV_{AS}/R_S$, and $\overline{V}_A = V_A/V_{AS}$ and where $\overline{u} = u/V_{AS}$ is the nondimensional radial wind speed; $M_{AS} \equiv u_S/V_{AS}$. Note that the system of equations (41)–(42) possesses a singularity at the Alfvén critical point $\overline{r}_A$, where the local Alfvén and the background wind speeds are equal. *Heinemann and Olbert* [1980] showed that there exists a regular solution, which smoothly passes through $\overline{r}_A$, corresponding to a local, purely outward propagating wave; this resolves the singularity. The regular solution at the Alfvén critical point $\overline{r} = \overline{r}_A$ must satisfy the condition [*Lou,* 1993a]

$$\overline{j} = -\frac{M_{AS}(\overline{\sigma}+2\overline{u}/\overline{r})\overline{\xi}}{\overline{\sigma}+d\overline{u}/d\overline{r}}\ , \tag{43}$$

which we enforce at $\overline{r}_A$ in our calculations.

As in the static case we have analyzed the propagation properties of Alfvén waves through the solar wind. To compute the transmission coefficient $\mathcal{T}$, we again placed a homogeneous layer (characterized by constant Alfvén speed) directly below the base of the transition region.

For the upper boundary we note that the flow problem is distinctly different from the static case: In the wind case there can exist inward propagating waves relative to the wind for any frequency at large distances from the Sun. In particular, one can define a characteristic angular frequency $\overline{\omega}_0 \equiv 1/(2M_A)$, which separates solutions at large distances into two qualitatively different classes [*Heinemann and Olbert,* 1980; *Barkhudarov,* 1991; *Lou,* 1993a]. For typical solar wind conditions the oscillation timescale corresponding to $\overline{\omega}_0$ ranges from ~ 15 to ~ 40 hours. For $\omega > \overline{\omega}_0$ there is a relatively small flux of inward propagating waves (relative to the wind), which vanishes at very high frequencies; for $\omega < \overline{\omega}_0$, no Alfvén waves propagate at asymptotically large $\overline{r}$, and a standing wave pattern relative to the wind is generated. As a consequence we cannot use the WKB approximation far from the Sun for all frequencies in order to define a transmission coefficient $\mathcal{T}$, and we have to reconsider the asymptotic boundary condition as appropriate.

V93 suggested a clever solution to this problem: Following his lead, we define the transmission coefficient by imposing the condition that waves at the Alfvén critical point are purely outwardly propagating; hence, (41) and (42) behave regularly at this point. This approach then provides the transmission and reflection properties of the sub–Alfvénic layer bounded by the solar surface below and by the Alfvén critical point above and thus allows us to compute the fraction of the incident wave flux that reach the super–Alfvénic wind. This approach would seem to be insufficient for the problem at hand, which is to compute the global transmission and reflection properties of the wind, as seen from the wind base. In particular, this approach does not take into account any further wave reflection that may take place in the super–Alfvénic wind. V93 recognized, however, that this discrepancy does not matter: A fundamental property of the super–Alfvénic wind is that inward propagating waves propagate more slowly toward the Sun than do the plasma outflows, so that these waves experience a net outward advection. As a consequence, waves reflected in the super–Alfvénic region cannot propagate back to the sub–Alfvénic portion of the wind and therefore cannot reach the solar surface. Thus these reflected waves do not provide any net contribution to the wind's overall transmission and reflection characteristics, and the transmission coefficient as defined just above suffices to define not only the propagation properties of the sub–Alfvénic wind, but also the global wind propagation properties as seen from the wind base.

As in the static case, we adopt two different methods to compute $\mathcal{T}$ in order to check our results. Since the net wave energy flux is not a conserved quantity in the presence of the solar wind (cf. equation (16)), we appeal instead to the conservation of wave action flux, written in the form (V93)

$$\mathcal{S}^+ - \mathcal{S}^- = \mathcal{S}_\infty \ , \qquad \mathcal{S}^\pm = \rho r^2 \frac{(u \pm V_A)^2}{V_A} \frac{|\mathbf{z}^\pm|^2}{8} \ , \tag{44}$$

where the plus and minus sign indicate the outward and inward wave action fluxes, respectively, and $\mathcal{S}_\infty$ is a constant. In analogy to the static case the transmission coefficient is defined as $\mathcal{T} \equiv \mathcal{S}_A^+/\mathcal{S}_S^+$, where $\mathcal{S}_S^+$ is the outgoing wave action flux at the base of the transition region and $\mathcal{S}_A^+$ is the outgoing wave action flux at the effective upper boundary of the inhomogeneous layer, i.e., the Alfvén critical point $\overline{r}_A$.

An alternative way to compute $\mathcal{T}$ is similar to that used by LR94 in the static case and described in the previous section. The main difference in the present case is that we now numerically integrate the wave equations backward to the solar surface, starting from the Alfvén critical point with the condition of purely outward propagating waves imposed. Near the solar surface, where the wind speed is very subsonic ($\sim 10^3$ cm s^{-1}), we can use the approximate solution of the static case; thus, at the base of the transition region we match the analytical solution (33) obtained in the base homogeneous medium to the numerical solutions computed in the inhomogeneous overlying atmosphere.

The parameters for the solar wind model considered here are listed in Table 1. The values of the proton number density and the flow velocity yield a solar mass loss rate $\dot{M} \sim 3.3 \times 10^{-14}\ M_S$ yr^{-1}, consistent with observations [see *Withbroe*, 1988]. Figure 4 shows the profiles of temperature T, velocity u and density n_p of the wind model. The local isothermal sound speed $c_s = [2k_BT/(\mu m_H)]^{1/2}$ and the Alfvén speed V_A are marked by dotted and dashed lines, respectively. The heliocentric radii of the sonic critical point (where the flow velocity is equal to c_s) and of the Alfvén critical point are roughly 2.0 and 34 solar radii, respectively.

We display the variation of the transmission coefficient $\mathcal{T}$ as a function of the wave period in Figure 5. As in the static case (Figure 1) there is a strong dependence of the transmission coefficient on the wave period for periods longer than 0.1 s, while for smaller periods the waves are totally transmitted. We also note that for short–period waves the present transmission coefficient is very similar in shape to the "static" transmission coefficient; in particular, the minimum in transmission occurs at a period of roughly 1 hour. In contrast, the present transmission coefficient is quite different from that for the static case at long periods ($> 10^3$ hours); transmission is relatively enhanced in the wind case. Note that $\mathcal{T}$ tends to a constant value for periods longer than 10^3 hours. This behavior was also found and extensively discussed by V93 for isothermal wind models. Figure 6 shows the consequence of this variation of transmission coefficient with wave period on the fluctuation power spectrum; we compare the power spectrum at the base of the transition region to that beyond the Alfvén critical radius. We note that for wave period P in the range 1 min $\lesssim P \lesssim$ 10 hours, the spectrum is steepened, while for $P \lesssim$ 1 min, it is flattened.

To understand the reason underlying the difference in transmission properties at lower frequencies, we appeal to the rough estimate of $\mathcal{T}$ discussed in the static case. We do note, however, that the critical angular frequency (39) is, strictly speaking, only properly defined in the case of a static background; hence our discussion is physically well motivated in the wind case only very close to the Sun, where the flow speed is subsonic. As a result our estimation of the transmission coefficient based on the critical frequency is least reliable for lower–frequency waves, because r_ω (which is the radius above which these wave propagate) is large and tends to lie in regions where the wind Mach number is not small compared to unity. We proceed as in the static case: Waves with period shorter than 0.1 s are totally transmitted, because their frequency is higher than the maximum critical frequency. As the wave period is increased, the point r_ω moves outward, and the thickness δ of the evanescent layer increases. The Alfvén speed at r_ω initially increases, reaching its maximum at a period of roughly 1 hour; the transmission coefficient shows a corresponding decrease in this interval, also reaching its minimum value at a period of 1 hour. Subsequent increases in the wave period lead to a decrease in the Alfvén speed and to a corresponding increase in the transmission coefficient.

The analogy with the static case we have been pursuing is possible only as long as r_ω is smaller than the Alfvén critical point radius r_A. If this inequality is violated, the static and wind cases behave quite differently. In particular, if the wave period is long enough so that $r_\omega > r_A$, the thickness of the evanescent layer for the wind case no longer increases and is instead bounded from above by the value $\delta_{max} \equiv r_A - R_S$. (The reason for this behavior is the trivial one that all waves propagate outward for $r > r_A$.) As a consequence the transmission coefficient (40) approaches the value

$$\mathcal{T} = \frac{4V_{AS}V_{Ac}}{(V_{AS}+V_{Ac})^2} \tag{45}$$

at long periods, where V_{Ac} is the Alfvén speed at the Alfvén critical point. Note that the position of the transmission minimum coincides in the static and expanding cases, because the Alfvén velocity at the base is the same in both cases. On the other hand, the value of $\mathcal{T}$ at the minimum differs in these two cases because the two Alfvén speed profiles differ. In particular, the maximum Alfvén speed is smaller in the presence of the wind than in the static case.

We conclude that the presence of the wind affects the propagation properties of Alfvén waves in the solar atmosphere primarily for waves with long periods. The physical reason for this behavior is that long–period waves reflected in the super–Alfvénic region cannot return to the sub–Alfvénic region, and hence to the solar surface, but are instead inevitably advected outward [see also *Hollweg,* 1996]. As a consequence, such waves can never show substantial reflection, as seen from the atmosphere's base.

7 Discussion and Conclusion

We have analyzed the transmission properties of the Alfvén waves in both static and expanding atmospheres, starting from the base of the transition region, where these waves most likely originate. Since we expect that the wind structure is affected by the total contribution of all the waves that propagate in the wind, our work takes into account the effects of momentum deposition due to a spectrum of both WKB and non–WKB waves.

We have used two different methods to compute the transmission coefficient of the waves through the solar atmosphere (V93, LR94), showing that they yield mutually consistent results.

In all cases we find an interesting feature in the transmission properties, namely, a transmission minimum at a period of roughly 1 hour. In order to find an intuitive explanation for this phenomenon we resorted to the critical frequency approach of *Musielak et al.,* [1992], who showed that the critical frequency Ω_{cr} allows one to define an evanescent layer for wave propagation in the solar atmosphere; by roughly evaluating the transmission coefficient of waves propagating in this layer we are able to explicate the variation of the transmission coefficient with wave period for both the static and wind cases on the basis of relatively straightforward physical grounds: It turns out that the wave propagation characteristics are basically determined by the values of the Alfvén speeds at the inner and outer boundaries of the evanescent layer; in particular, transmission is high when these two speeds are similar in value and low when they are very different. This description suggests that Alfvén wave propagation through the evanescent layer may be looked at as an "impedance matching" problem: Tunneling (and thus high transmission) occurs only when the transmission speeds match at either end of the transmission barrier.

It is interesting to compare our results with those obtained by V93 and LR94 in the simpler case of an isothermal static atmosphere. These authors analyzed the behavior of the transmission coefficient as a function of the wave frequency and of the nondimensional parameter $\alpha = GM_*/R_* c_s^2$, where M_* and R_* are the mass and the radius, respectively, of the star and c_s is the isothermal sound speed (α is just the inverse pressure scale height at the stellar surface, scaled to the stellar radius; $H_{p*} \equiv k_B T_*/(\mu m_H) \cdot (GM_*/R_*^2)^{-1} = R_*/\alpha$; there is a typo of factor 2 in the LR94 calculations). In particular, they found (for $M_* = M_S$, $R_* = R_S$) that the transmission coefficient increases monotonically with wave frequency if the temperature of the isothermal atmosphere is of the order of, or larger than, 2×10^6 K, while a minimum appears at lower temperatures. The resulting variation of their transmission coefficient with frequency is very similar to what we find: The minimum at lower temperature is due to the steepening of the gradient of the Alfvén speed near the Sun, which enhances the reflection at intermediate frequencies; similarly, in our background atmosphere model, waves of intermediate frequency experience significant reflection due to the very steep gradient of the Alfvén speed present in the transition region.

It is now straightforward to explain the differences between our transmission coefficients and those computed by V93 for coronal temperatures in the range 8×10^5 to 3×10^6 K. The key point is the radial structure of the Alfvén speed profile. In the isothermal models of V93 the radial profile of V_A depends on the temperature of the atmosphere, with the position of the V_A maximum related to the temperature via the relation $\overline{r} = \alpha/4$. In particular, the maximum lies at the solar surface if the temperature is equal to, or higher than, 3×10^6 K. In contrast, if the temperature is decreased, the position of the V_A maximum moves outward, and the value of V_A increases with respect to its value at the base; as a result a minimum in the transmission coefficient appears, which becomes more prominent as the temperature is lowered further. Our model of the background atmosphere takes into account the transition region and therefore shows a much more rapid decrease of the density just above the surface than is the case for the model of V93. As a consequence the Alfvén speed increases much more quickly in our model, reaching its maximum value at $\sim 2\ R_S$, so that the transmission coefficient has its minimum at a period around 1 hour.

We are also able to explain the apparent disagreement (discussed by LR94) between the results of LR94 and the results of *Similon and Zargham* [1992] (hereinafter referred to as SZ92). SZ92 considered an open magnetic structure emerging from the Sun, and they focused on the rapid expansion of the magnetic flux tube in the chromosphere and transition region. They found wave transmission in their computation to lie in a range between 5% and 30%, whereas LR94 found transmission coefficients greater than 30% at high frequencies. In light of our results we interpret this difference as being due to the different profiles of the Alfvén speed in the two models. In particular, SZ92 considered wave propagation in the chromosphere and transition region, where a steep gradient of Alfvén speed is present. The difference between the Alfvén speed at the two boundaries of their evanescent layer is very large, and we therefore expect very significant wave reflection. In contrast, LR94 started their solar models slightly above the transition region, where the temperature is greater than $\sim 10^6$ K and the Alfvén speed varies slowly; their model therefore does not show as large a difference in Alfvén speed at the inner and outer boundaries of their evanescent layer, and as a result, Alfvén waves are transmitted more efficiently in the model of LR94 than in that of SZ92.

Because our background model includes the transition region, we are in a position to conduct a better comparison with the model of SZ92. Indeed, our value for the minimum value for the transmission coefficient (about 10%) is bracketed by the values obtained by SZ92 for an axisymmetric structure with a magnetic flux tube expansion factor of 40 ($\mathcal{T} \sim 1\%$ at a wave period of 1 hour) and 400 ($\mathcal{T} \sim 30\%$ at the same wave period). The differences in transmission properties in the calculations of SZ92 are due in part to the different expansion rates of their flux tubes (which are completely radial in our model) and in part to the different boundary conditions at the base of the models (SZ92 start their models at the photosphere, while we start our models in the lower transition region); as a consequence, both the detailed Alfvén speed profiles and the base values of the Alfvén speed are different.

Next, we note that *MacGregor and Charbonneau* [1994] have also considered the propagation of Alfvén waves in an expanding wind. While our computational approach is similar to theirs, our basic physical assumptions differ considerably. In particular, their calculations are based on an isothermal background wind, while our calculations allow for radial temperature variations; they considered momentum deposition by monochromatic waves, while we allowed for a wide spectrum of non–WKB Alfvén waves. These authors analyzed wave reflection for waves of different frequencies; among other results they found that waves at frequencies $\omega \sim 10^{-3}$ s^{-1} (i.e., close to the minimum in transmission shown in Figure 5) undergo larger reflection close to the solar surface than they do further away. Our analysis shows why: Adopting their notation, we plot the ratio $|F|^2/|G|^2$ of the squared moduli of the reflected wave amplitude to the transmitted wave amplitude (Figure 7), where

$$
\begin{aligned}
|F|^2 &= \frac{(u-V_A)^2}{uV_A}|\mathbf{z}^-|^2 , \\
|G|^2 &= \frac{(u+V_A)^2}{uV_A}|\mathbf{z}^+|^2 .
\end{aligned}
\tag{46}
$$

Figure 7 shows that waves with period $P = 1$ hour (e.g., corresponding to the transmission minimum in Figure 5, and close to the frequency considered by *MacGregor and Charbonneau* [1994]) are reflected considerably more efficiently near the transition region than further out and that this contrast in reflection efficiencies is much smaller at lower frequencies (longer periods).

Finally, we note that the frequency of the transmission minimum depends on the boundary conditions at the base. That is, the critical frequency Ω_{cr} (equation (39)) depends on the base Alfvén speed V_{AS} and on the solar radius R_S: If V_{AS} is increased, then Ω_{cr} will increase as well, and higher–frequency waves will be reflected. As a result the curve in Figure 1 would be shifted to the right as V_{AS} is increased. The transmission minimum (at a period of roughly 1 hour for conditions characteristic of the model used in this paper) is therefore dependent on the boundary conditions selected at the presumed source region of the waves; put slightly differently, the dependence of the transmission coefficient on the wave period or frequency is determined by the physical conditions in the region where the waves originate. In this paper we have simply assumed that we know where this source region is located (namely, in a region corresponding to a base proton number density of $\sim 10^{10}$ cm^{-3} and a base magnetic field of ~ 10 G, chosen at a base temperature of $\sim 2 \times 10^4$ K). It will be extremely interesting to use coronal and interplanetary observations to infer these base conditions from the emergent wave spectrum (using calculations of the sort presented here) and then to compare these inferences with observations of waves at the base of the solar atmosphere.

Acknowledgments. We are grateful to V. Hansteen, T. E. Holzer, E. Leer, F. Reale, and S. Serio for useful discussions as well as to two anonymous referees for useful criticisms and suggestions. SO acknowledges the hospitality of the Department of Astronomy and Astrophysics, University of Chicago, where most of the present work was carried out. This work was supported in part by Ministero della Università e della Ricerca Scientifica e Tecnologica and GNA-CNR and in part by NSF and NASA grants to the University of Chicago.

The Editor thanks J. V. Hollweg and A. V. Usmanov for their assistance in evaluating this paper.

References

Alazraki, G., and P. Couturier, Solar wind acceleration caused by the gradient of Alfvén wave pressure, *Astron. Astrophys. J., 13*, 380, 1971.

An, C.–H., Z. E. Musielak, R. L. Moore, and S. T. Suess, Reflection and trapping of transient Alfvén waves propagating in an isothermal atmosphere with constant gravity and uniform magnetic field, *Astrophys. J., 345*, 597, 1989.

An, C.–H., S. T. Suess, R. L. Moore, and Z. E. Musielak, Reflection and trapping of Alfvén waves in spherically symmetric stellar atmosphere, *Astrophys. J., 350*, 309, 1990.

Balogh, A., E. J. Smith, B. T. Tsurutani, D. J. Southwood, R. J. Forsyth, and T. S. Horbury, The heliospheric magnetic field over the south polar region of the Sun, *Science, 268*, 1007, 1995.

Barkhudarov, M. R., Alfvén waves in stellar winds, *Sol. Phys., 135*, 131, 1991.

Barnes, A., Theory of magnetohydrodynamic waves: The WKB approximation revisited, *J. Geophys. Res., 97*, 12,105, 1992.

Belcher, J. W., Alfvénic wave pressures and the solar wind, *Astrophys. J., 168*, 509, 1971.

Belcher, J. W., and L. Davis Jr., Large–amplitude Alfvén waves in the interplanetary medium, 2, *J. Geophys. Res., 76*, 3534, 1971.

Belcher, J. W., and S. Olbert, Stellar winds driven by Alfvén waves, *Astrophys. J., 200*, 269, 1975.

Belcher, J. W., L. Davis Jr., and E. J. Smith, Large–amplitude Alfvén waves in the interplanetary medium: Mariner 5, *J. Geophys. Res., 74*, 2302, 1969.

Bray, R. J., and R. E. Loughhead, *The Solar Chromosphere*, Chapman and Hall, New York, 1974.

Coleman, P. J., Jr., Turbulence, viscosity and dissipation in the solar wind plasma, *Astrophys. J., 153*, 371, 1968.

Elsässer, W. M., The hydromagnetic equations, *Phys. Rev., 79*, 183, 1950.

Ferraro, V. C. A., On the reflection and refraction of Alfvén waves, *Astrophys. J., 119*, 393, 1954.

Ferraro, V. C. A., and C. Plumpton, Hydromagnetic waves in a horizontally stratified atmosphere, *Astrophys. J., 127*, 459, 1958.

Goldstein, M. L., D. A. Roberts, and W. H. Matthaeus, Magnetohydrodynamic turbulence in the solar wind, *Annu. Rev. Astron. Astrophys., 33*, 283, 1995.

Grall R. R., W. A. Coles, M. T. Klinglesmith, A. R. Breen, P. J. S. Williams, Jussi Markkanen, and Ruth Esser, Rapid acceleration of the polar solar wind, *Nature, 379*, 429, 1996.

Heinemann, M., and S. Olbert, Non–WKB Alfvén waves in the solar wind, *J. Geophys. Res., 85*, 1311, 1980.

Henyey, L. G., J. E. Forbes, and N. L. Gould, A new method of automatic computation of stellar evolution, *Astrophys. J., 139*, 306, 1964.

Hollweg, J. V., Alfvén waves in the solar wind: Wave pressure, Poynting flux, and angular momentum, *J. Geophys. Res., 78*, 3643, 1973.

Hollweg, J. V., Some physical processes in the solar wind, *Rev. Geophys., 16*, 689, 1978a.

Hollweg, J. V., Alfvén waves in the solar atmosphere, *Sol. Phys., 56*, 305, 1978b.

Hollweg, J. V., On WKB expansions for Alfvén waves in the solar wind, *J. Geophys. Res., 95*, 14,873, 1990.

Hollweg, J. V., Non–WKB Alfvén waves in the solar wind: Propagation and reflection of pulses, in *Solar Wind Eight*, in press 1996.

Holzer, T. E., Effects of rapidly diverging flow, heat addition, and momentum addition in the solar wind and stellar winds, *J. Geophys. Res., 82*, 23, 1977.

Holzer, T. E., T. Flå, and E. Leer, Alfvén waves in stellar winds, *Astrophys. J., 275*, 808, 1983.

Jacques, S. A., Momentum and energy transport by waves in the solar atmosphere and solar wind, *Astrophys. J., 215*, 942, 1977.

Krogulec, M., Z. E. Musielak, S. T. Suess, S. F. Nerney, and R. L. Moore, Reflection of Alfvén waves in the solar wind, *J. Geophys. Res., 99*, 23, 489, 1994.

Lau, Y.–T., and E. Siregar, Nonlinear Alfvén wave propagation in the solar wind, *Astrophys. J., 465*, 451, 1996.

Leer, E., T. E. Holzer, and T. Flå, Acceleration of the solar wind, *Space Sci. Rev., 33*, 161, 1982.

Leroy, B., Propagation of waves in an atmosphere in the presence of a magnetic field, *Astron. Astrophys., 91*, 136, 1980.

Lou, Y.–Q., Three–dimensional magnetic field configurations in the heliosphere, *J. Geophys. Res., 97*, 17,183, 1992.

Lou, Y.–Q., Propagation of three–dimensional Alfvén waves and its nonlinear effects in the solar wind, *J. Geophys. Res., 98*, 3563, 1993a.

Lou, Y.–Q., Three–dimensional nonsteady compressible magnetohydrodynamic fluctuations in the solar wind, *J. Geophys. Res., 98*, 11,483, 1993b.

Lou, Y.–Q., Compressible fluctuations in the equatorial solar wind with a spiral magnetic field, *J. Geophys. Res., 99*, 8491, 1994a.

Lou, Y.–Q., Alfvénic disturbances in the equatorial solar wind with a spiral magnetic field, *J. Geophys. Res., 99*, 14,747, 1994b.

Lou, Y.–Q., On two–component models of solar wind fluctuations, *J. Geophys. Res., 100*, 5877, 1995.

Lou, Y.–Q., Corotating shock accelerated particles guided by wavy spiral magnetic fields in the solar wind at high heliographic latitudes, *Geophys. Res. Lett., 23*, 609, 1996.

Lou, Y.–Q., and R. Rosner, Reflection of Alfvén waves in stellar atmospheres: The case of open magnetic fields, *Astrophys. J., 424*, 429, 1994.

MacGregor, K. B., and P. Charbonneau, Stellar winds with non–WKB Alfvén waves, I, wind models for solar coronal conditions, *Astrophys. J., 430*, 387, 1994.

Moore, R. L., Z. E. Musielak, S. T. Suess, and C.–H. An, Alfvén wave trapping, network microflaring, and heating in solar coronal holes, *Astrophys. J., 378*, 347, 1991.

Musielak, Z. E., J. M. Fontenla, and R. L. Moore, Klein–Gordon equation and reflection of Alfvén waves in nonuniform media, *Phys. Fluids B, 4*, 13, 1992.

Parker, E. N., Dynamics of the interplanetary gas and magnetic fields, *Astrophys. J., 128*, 664, 1958.

Parker, E. N., *Interplanetary Dynamical Processes*, Wiley Interscience, New York, 1963.

Parker, E. N., Dynamical theory of the solar wind, *Space Sci. Rev., 4*, 666, 1965.

Parker, E. N., Heating solar coronal holes, *Astrophys. J., 372*, 719, 1991.

Phillips, J. L., S. J. Bame, W. C. Feldman, B. E. Goldstein, J. T. Gosling, C. M. Hammond, D. J. McComas, M. Neugebauer, E. E. Scime, and S. T. Suess, Ulysses solar wind plasma observations at high southerly latitudes, *Science, 268*, 1030, 1995.

Press, W. H., B. P. Flannery, S. A. Teukolsky, and W. T. Vetterling, *Numerical Recipes*, Cambridge Univ. Press, New York, 1986.

Raymond, J. C., and B. W. Smith, Soft X–ray spectrum of a hot plasma, *Astrophys. J., 35*, suppl. 419, 1977.

Roberts, D. A., and M. L. Goldstein, Turbulence and waves in the solar wind, *U.S. Natl. Rep. Int. Union Geod. Geophys. 1987–1990, Rev. Geophys., 29*, 932, 1991.

Rosner, R., W. H. Tucker, and G. S. Vaiana, Dynamics of quiet solar corona, *Astrophys. J., 220*, 643, 1978.

Rosner, R., B. C. Low, and T. E. Holzer, Physical properties in the solar corona, in *Physics of the Sun*, vol. 2, edited by P. A. Sturrock, T. E. Holzer, D. M. Mihalas, and R. K. Ulrich, chap. 11, pp. 135–180, D. Reidel, Norwell, Mass., 1986.

Rosner, R., C.–H. An, Z. E. Musielak, R. L. Moore, and S. T. Suess, Magnetic confinement, Alfvén wave reflection, and the origins of X–ray and mass–loss "dividing lines" for late–type giants and supergiants, *Astrophys. J. Lett., 372*, L91, 1991.

Similon, P. L., and S. Zargham, Alfvén wave transmission through the solar atmosphere, *Astrophys. J., 388*, 644, 1992.

Smith, E. J., A. Balogh, R. P. Lepping, M. Neugebauer, J. Phillips, and B. T. Tsurutani, Ulysses observations of latitude gradients in the heliospheric magnetic field: Radial component and variances, *Space Sci. Rev., 72*, 165, 1995.

Spitzer, L., *Physics of Fully Ionized Gases*, Wiley Interscience, New York, 1962.

Tu, C.–Y., and E. Marsch, *MHD Structures, Waves and Turbulence in the Solar Wind: Observations and Theories*, Kluwer Acad., Norwell, Mass., 1995.

Velli, M., On the propagation of ideal, linear Alfvén waves in radially stratified stellar atmospheres and winds, *Astron. Astrophys., 270*, 304, 1993.

Withbroe, G. L., The temperature structure, mass, and energy flow in the corona and inner solar wind, *Astrophys. J., 325*, 442, 1988.

Table 1: Parameters for the static and wind models described in sections 5 and 6, respectively. Variables are as follows: T_S, temperature; n_{pS}, proton number density; u_S, radial flow speed; B_S, radial magnetic field strength; H_S, volumetric heating rate at the base of the transition region; λ_H, heating scale length; and T_{max} maximum of the temperature.

	Static	Wind
$T_\odot$ (K)	2×10^4	2×10^4
$n_{p\odot}$ (cm^{-3})	10^{10}	5×10^9
$u_\odot$ (cm s^{-1})	0	3.3×10^3
$B_\odot$ (G)	10	10
$H_\odot$ (erg cm^{-3} s^{-1})	1.3×10^{-6}	2.0×10^{-6}
λ_H (cm)	6.96×10^{10}	6.96×10^{10}
T_{max} (K)	1.9×10^6	1.4×10^6

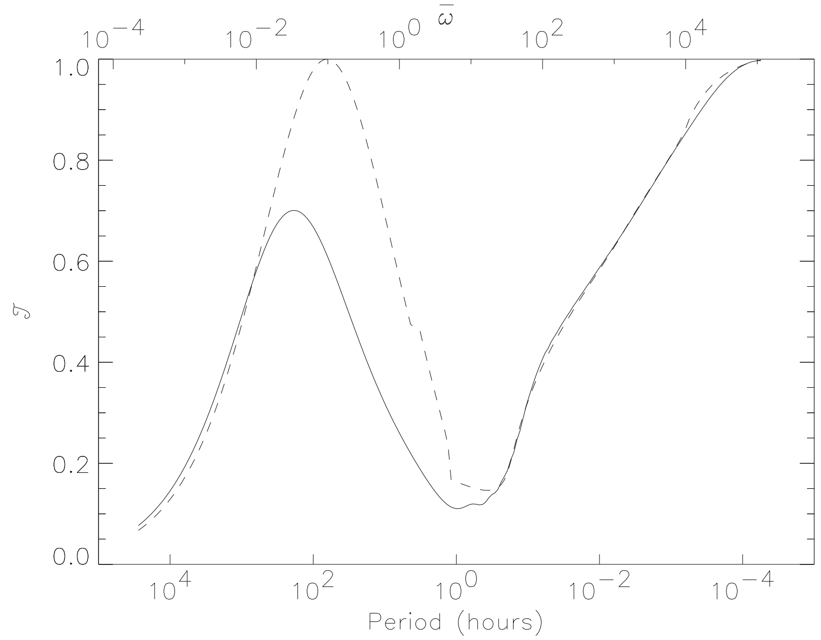

Figure 1: Alfvén wave transmission coefficient versus wave period for the static background solar atmosphere (solid line). The dashed line is a rough estimate of the transmission coefficient computed under the assumption that the mode wavelength is longer than the thickness of the evanescent layer (see text). The upper horizontal axis shows the nondimensional frequency $\overline{\omega} = \omega R_S/V_{AS}$.

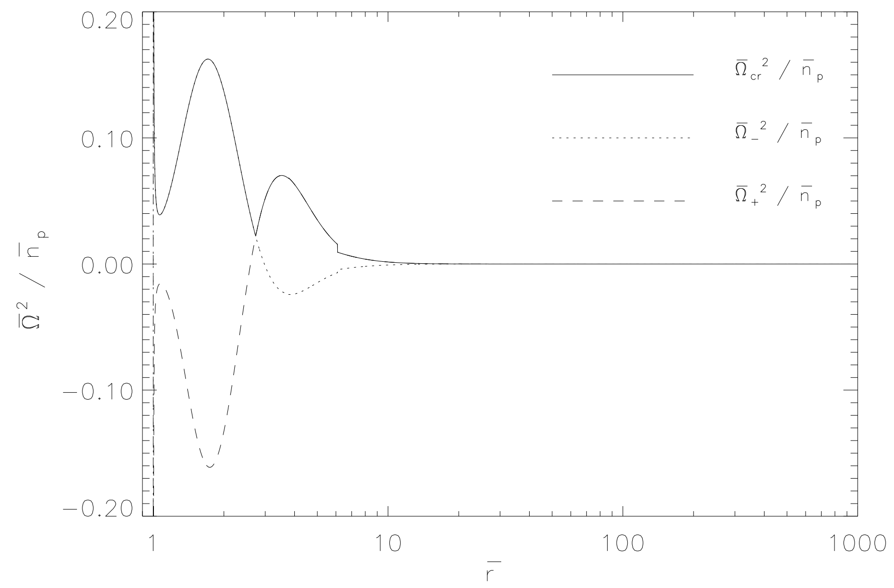

Figure 2: Ratios of the squares of the normalized characteristic frequencies $\overline{\Omega}_{\mp} = \Omega_{\mp} R_S/V_{AS}$ (cf. equation 38) and $\overline{\Omega}_{cr} = \Omega_{cr} R_S/V_{AS}$ (cf. equation 39) to the normalized proton number density $\overline{n}_p = n_p/n_{pS}$ versus $\overline{r}$, the heliocentric distance normalized to the solar radius.

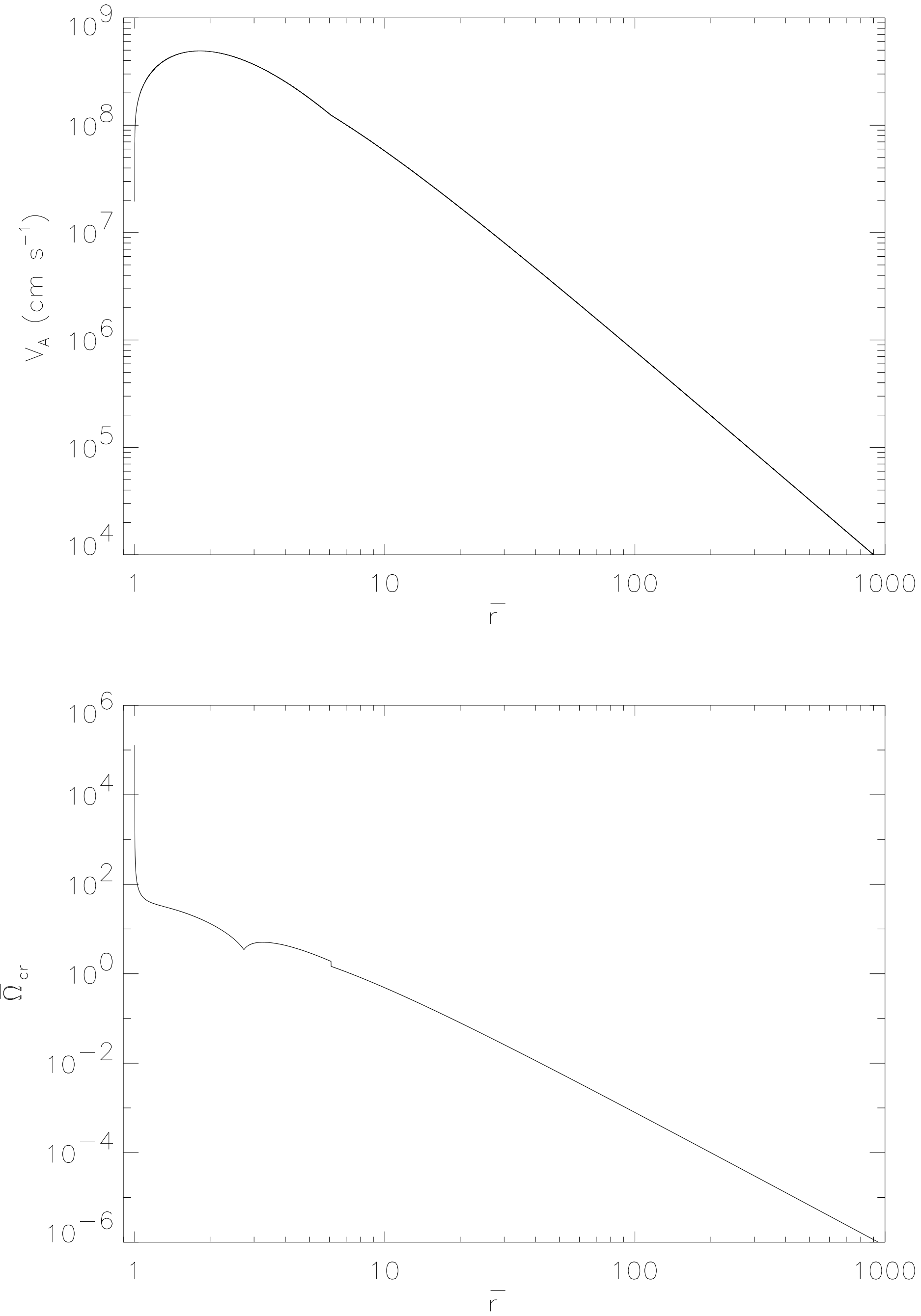

Figure 3: (top) Alfvén wave speed V_A and (bottom) normalized critical frequency $\overline{\Omega}_{cr} = \Omega_{cr} R_S / V_{AS}$ versus $\overline{r}$, the heliocentric distance normalized to the solar radius, for the static background solar atmosphere.

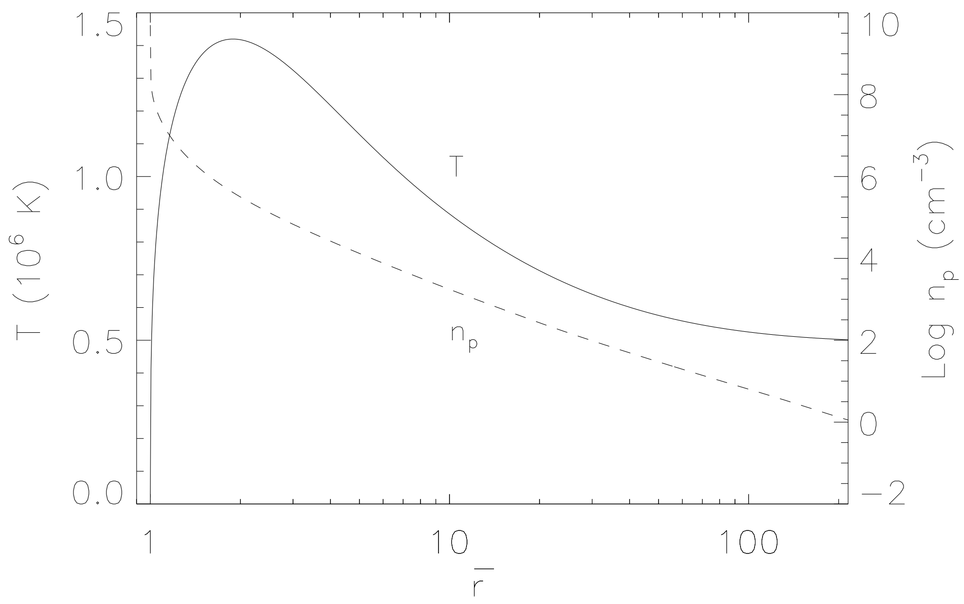

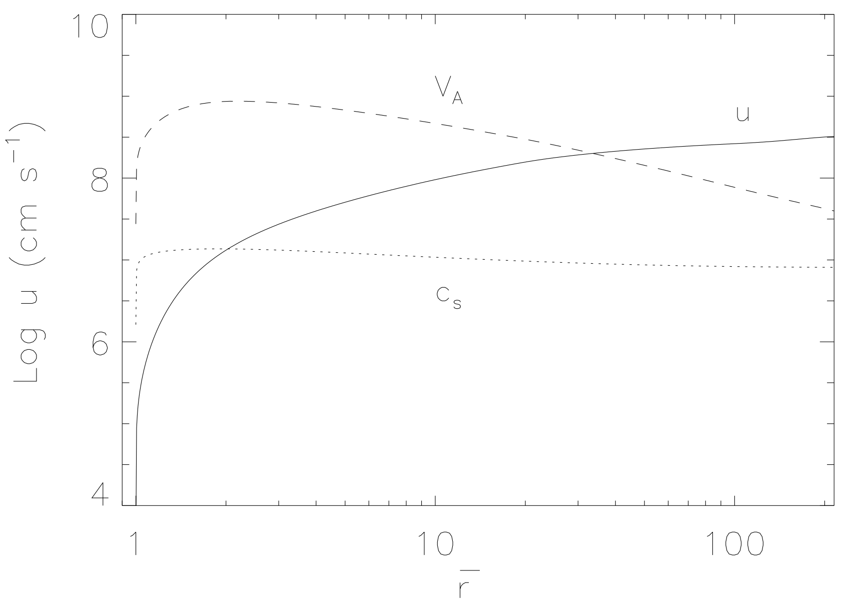

Figure 4: (top) Temperature T (solid line) and density n_p (dashed line) versus the heliocentric distance normalized to the solar radius $\overline{r}$ in our solar wind model. (bottom) Wind velocity u (solid line), local isothermal sound speed c_s (dotted line), and Alfvén speed V_A (dashed line) versus $\overline{r}$.

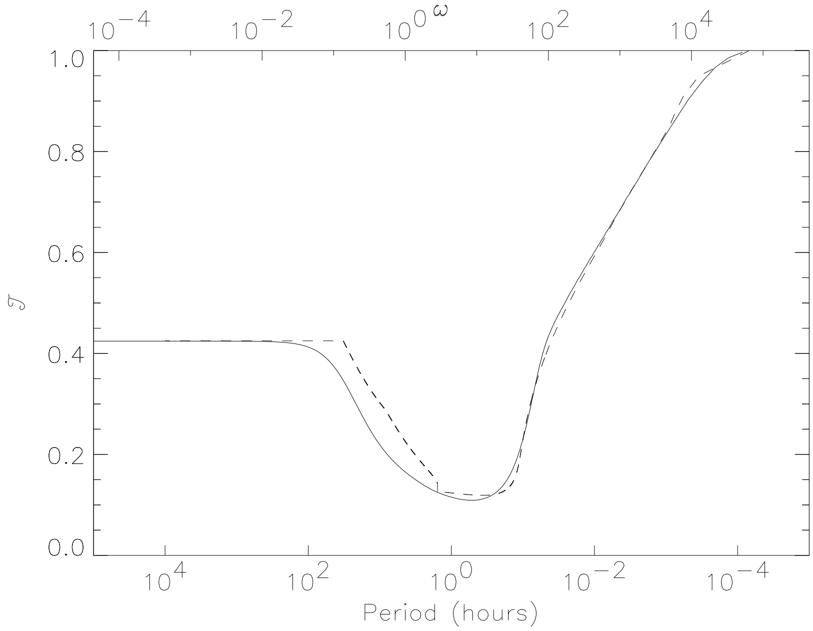

Figure 5: As in Figure 1, but in the presence of the wind.

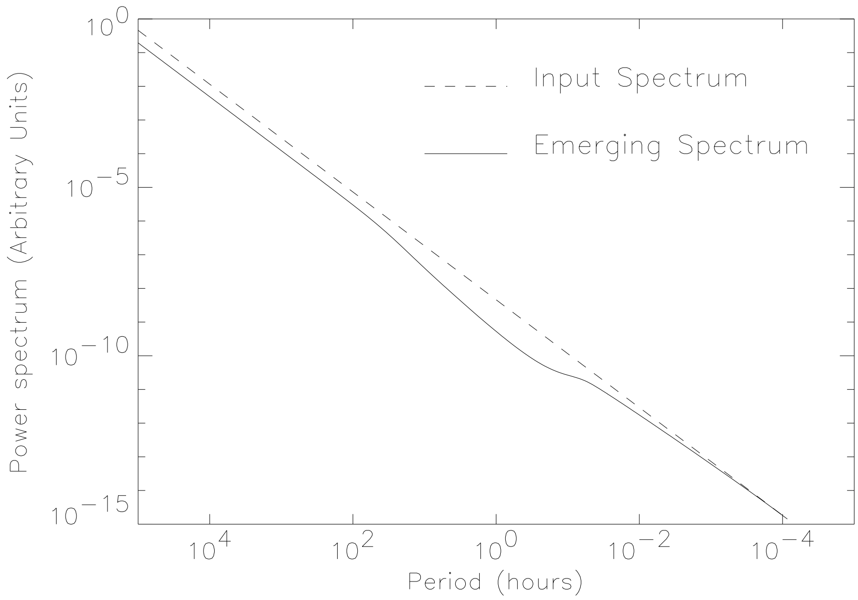

Figure 6: Comparison of the input and emergent power spectra for Alfvén waves in the background wind. The input spectrum obtains at the base of the transition region; the emergent spectrum is evaluated beyond the Alfvén critical point.

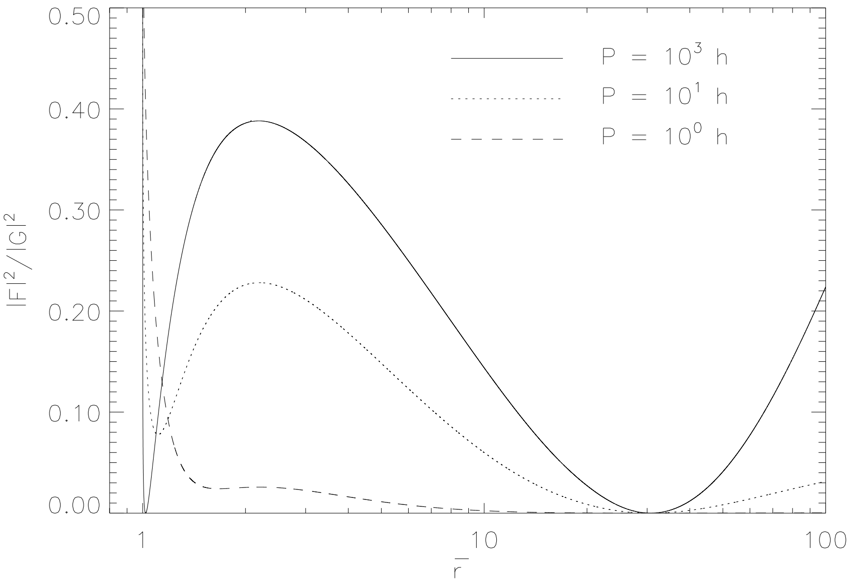

Figure 7: Ratios of the squared moduli of the reflected wave amplitude to the transmitted wave amplitude, plotted versus normalized heliocentric distance, for wave periods $P = 10^3$, 10, and 1 hours.